Progress in Oceanography 172 (2019) 65–76

Contents lists available at ScienceDirect

Progress in Oceanography

journal homepage: www.elsevier.com/locate/pocean

Insights into carbon acquisition and photosynthesis in *Karenia brevis* under a range of CO_2 concentrations

T.L. Bercel*, S.A. Kranz

Department of Earth, Ocean and Atmospheric Science, Florida State University, Tallahassee, FL 32306, USA

ARTICLE INFO

Keywords:
Red tides (RT Algal Blooms)
Carbon fixation (RT photosynthesis)
Neurotoxins
Acidification (RT pH)
Climate change
Carbon concentrating mechanism
Regional USA
Gulf of Mexico
Florida

ABSTRACT

Karenia brevis is a marine dinoflagellate commonly found in the Gulf of Mexico and important both ecologically and economically due to its production of the neurotoxin brevetoxin, which can cause respiratory illness in humans and widespread death of marine animals. *K. brevis* strains have previously shown to be sensitive to changes in CO_2, both in terms of growth as well as toxin production. Our study aimed to understand this sensitivity by measuring underlying mechanisms, such as photosynthesis, carbon acquisition, and photophysiology. *K. brevis* (CCFWC-126) did not show a significant response in growth, cellular composition of carbon and nitrogen, nor in photosynthetic rates between pCO_2 concentrations of 150, 400, or 780 µatm. However, a strong response in its acquisition of inorganic carbon was found. Half saturation values for CO_2 increased from 1.5 to 3.3 µM, inorganic carbon preference switched from HCO_3^- to CO_2 (14–56% CO_2 usage), and external carbonic anhydrase activity was downregulated by 23% when comparing low and high pCO_2. We conclude that *K. brevis* must employ an efficient and regulated CO_2 concentrating mechanism (CCM) to maintain constant carbon fixation and growth across pCO_2 levels. No statistically significant correlation between CO_2 and brevetoxin content was found, yet a positive trend with enhanced pCO_2 was detected. This study is the first explaining how this socioeconomically important species is able to efficiently supply inorganic carbon for photosynthesis, which can potentially prolong bloom situations. This study also highlights that elevated CO_2 concentrations, as projected for a future ocean, can affect underlying physiological processes of *K. brevis*, some of which could lead to increases in cellular brevetoxin production and therefore increased impacts on coastal ecosystems and economies.

1. Introduction

By the end of the 21st century, atmospheric CO_2 is expected to increase to 1000 µatm (Solomon et al., 2007). This increase in CO_2 will result in a reduction of seawater pH of up to 0.4 units, a process called 'ocean acidification'. In addition, a rise in temperature will result in a shoaling of the mixed layer, and a reduction in nutrient availability in the upper layer (Boyd and Doney, 2003). It has been speculated that dinoflagellates could become more abundant in the future ocean, as some species might benefit from projected changes in the marine environment. For example, dinoflagellates have the ability to swim and access nutrients below a shallower mixed layer (Glibert et al., 2005; Moore et al., 2008), use mixotrophic metabolic strategies to reduce dependency on inorganic nutrients (Stoecker et al., 2017), and could benefit from enhanced CO_2 concentrations directly. Yet, despite the importance of pelagic dinoflagellates in the marine environment, relatively few studies have focused on the response of this group to future environmental changes (e.g. Hansen et al., 2007; Fu et al., 2010; Eberlein et al., 2014; Hardison et al., 2014; Magaña and Villareal, 2006; Maier Brown et al., 2006; Errera et al., 2010; Lekan and Tomas, 2010; Errera and Campbell, 2011; Hardison et al., 2012, 2013; Errera et al., 2014; Hoins et al., 2016).

It is important to understand the response of marine pelagic photoautotrophic organisms to projected environmental changes, as these organisms make up the base of the marine food web and conduct important ecosystem functions. Over the last decades, responses of

Abbreviations: GoM, Gulf of Mexico; CCM, Carbon Concentrating Mechanism; RubisCO, Ribulose-1,5-bisphosphate carboxylase/oxygenase enzyme; PS, Photosystem; CA, Carbonic Anhydrase; C, Carbon; N, Nitrogen; Si, Silicon; O_2, Oxygen; CO_2, Carbon Dioxide; HCO_3^-, Bicarbonate; PO_4^{3-}, Phosphate; KSO_4, Potassium sulfate; DIC, Dissolved inorganic carbon; K_m, Half saturation concentration of RubisCO; $K_{1/2}$, Half saturation concentration of photosynthesis; GPP, Gross Primary Productivity; NPP, Net Primary Productivity; NPQ, Nonphotochemical quenching

* Corresponding author.
E-mail address: tbercel@fsu.edu (T.L. Bercel).

https://doi.org/10.1016/j.pocean.2019.01.011
Received 10 September 2018; Received in revised form 23 January 2019; Accepted 25 January 2019
Available online 28 January 2019
0079-6611/

phytoplankton to temperature, nutrient availability, CO_2, and ocean acidification have been characterized and found to be diverse and multifaceted (Langer et al., 2011; Hutchins et al., 2013; Schaum et al., 2013; Petrou et al., 2016; Mackey et al., 2015), varying even between strains of the same species (Schaum et al., 2013).

Obligate photoautotrophic organisms, such as many marine phytoplankton, require the inorganic forms of carbon (CO_2 or bicarbonate (HCO_3^-)) to build organic molecules such as sugars, amino acids, etc. The key enzyme for the conversion of CO_2 into organic carbon within the Calvin-Benson cycle is Ribulose-1,5-bisphosphate carboxylase/oxygenase (RubisCO). Different forms of RubisCO have evolved over time, which resulted in a range of efficiencies to utilize CO_2 (Raven et al., 2012; Tortell, 2000). Most photoautotrophic dinoflagellates contain a very inefficient type II RubisCO (Morse et al., 1995; Badger et al., 1998; Tortell, 2000). However, it has been found that some dinoflagellate species including the species of interest in this study, *Karenia brevis*, possess the more efficient type I RubisCO which is similar to that found in haptophytes (Yoon et al., 2005, 2002). *K. brevis* is thought to have acquired type I RubisCO via tertiary endosymbiosis of a haptophyte as phylogenetic studies based on RubisCO and photosystem I genes show a close relationship between *K. brevis* and the haptophytes *Emiliania huxleyi, Pavlova lutheri,* and *Prymnesium parvum* (Yoon et al., 2005, 2002). Thus, the physiological response of *K. brevis* to changes in CO_2 concentrations may be distinct to that of other dinoflagellates that contain type II RubisCO. Nonetheless, both type I and II RubisCO are inherently inefficient as all RubisCOs catalyze reactions for photorespiration using O_2 in addition to carbon fixation using CO_2. Its proclivity to catalyze either the carboxylation or oxygenation reaction represents a challenge for efficient carbon fixation in all photosynthetic organisms and is described as the substrate specificity factor (S_{rel}*). The substrate specificity factor for *Amphidinium carterae,* a dinoflagellate with type II RubisCO is relatively low (S_{rel}* of 37 in (Badger et al., 1998)), however, the type I RubisCO found in *K. brevis* potentially has a higher specificity factor (S_{rel}* of ~18 in *Pavlova lutheri* or 77–79 in *Emiliania huxleyi* (Badger et al., 1998, Heureux et al., 2017)). RubisCO also has a low affinity for CO_2, with half saturation concentrations (K_m) mostly higher than the CO_2 concentration found in ambient marine environments (K_m values of 6–185 μM in algae and between 14 and 114 in haptophytes and dinoflagellates) (Badger et al., 1998; Heureux et al., 2017; Tortell, 2000).

To compensate for the poor efficiency of RubisCO, most species evolved so-called CO_2 concentrating mechanisms (CCMs). In general, CCMs include pathways to increase the CO_2 concentration in the proximity of RubisCO compared to the concentration in the seawater. Processes include the active, energy dependent transport of HCO_3^- or facilitated transport of CO_2 into the cell, the presence of carbonic anhydrases (CAs; which speed up the slow interconversion of carbon species), the reduction of efflux of CO_2 from the cell back to the seawater, and specialized compartments in which RubisCO is concentrated, so called pyrenoids in eukaryotic algae or carboxysomes in cyanobacteria (Giordano et al., 2005; Raven and Johnston, 1991). Previous studies have found strong evidence for pyrenoids in *K. brevis* strains (Monroe et al., 2010), indicating that this species has structural components of a CCM. While a direct proof for the existence of a CCM is that the observed half saturation concentration of photosynthesis ($K_{1/2}$ (CO_2) is lower than the half saturation concentration of the RubisCO (Km (CO_2)) (Giordano et al., 2005), those particular mechanisms have not been investigated for *K. brevis* yet. The CCM can, in some instances, be a costly process since it requires the active, energy driven uptake of inorganic carbon and the expression of a variety of enzymes (e.g. transporters, CAs) (Giordano et al., 2005). Despite a potentially large energy and resource requirement, the net benefit usually outweighs the costs, as cells would otherwise have high photorespiration and low CO_2 fixation capability. It has been speculated that an increase in CO_2 concentration could potentially decrease the need for CCMs (e.g. acquire CO_2 via diffusive uptake rather than active pumping of HCO_3^-, reduced requirement to express CAs) (Mackey et al., 2015 and references within). This down-regulation could potentially allow for energy and resources to be allocated to other physiological processes, such as growth, nitrogen acquisition (Giordano et al., 2005; Rost et al., 2008; Kranz et al., 2011; Mackey et al., 2015), and likely the production of secondary metabolites such as toxins.

Despite the suggestion that dinoflagellates might benefit directly from enhanced dissolved CO_2 concentrations in a future ocean, cellular responses in carefully conducted CO_2 experiments indicate that responses are diverse. For example, Hoins et al. (2016) did not find any growth response to different low or high CO_2 concentrations in the dinoflagellates *Gonyaulax spinifera* (grown under low light), *Protoceratium reticulatum, Alexandrium fundyense,* and *Scrippsiella trochoidea* (grown under nitrogen limitation), yet this study found a decreased growth rate in *S. trochoidea* with increased CO_2 under nitrogen-replete conditions. Eberlein et al. (2014) demonstrated that the dinoflagellates *Alexandrium tamarense* and *S. trochoidea* were unaffected by changes in pCO_2 in their growth rates, yet *S. trochoidea* was sensitive to enhanced CO_2 in its elemental composition.

In our study, we investigated the responses and underlying key physiological processes of the dinoflagellate *K. brevis* to changes in CO_2 concentration. *K. brevis*, a photosynthetic marine dinoflagellate commonly found in Gulf of Mexico (GoM) waters, is capable of forming dense blooms, also known as red tides, and able to produce brevetoxins, a type of neurotoxin (Brand et al., 2012). Blooms of *K. brevis* occur annually in the GoM and are one of the most predictable harmful algal blooms on our planet (Heil et al., 2014). The production of brevetoxin results in mortality of marine mammals, fish, and other marine life, and also causes respiratory illness in humans (Landsberg, 2002; Flewelling et al., 2005). Hence, the occurrence of *K. brevis* blooms have large impacts on the local environment and human health, and have sizeable environmental and economic effects (Landsberg, 2002; Fleming et al., 2005; Hoagland et al., 2009).

Due to the impact of this species on the local economy and human health within the GoM it is necessary to assess how environmental changes will affect this species. Many studies on *K. brevis* have been conducted in order to understand how different environmental parameters can affect growth, productivity, and toxicity (Steidinger, 2009; Brand et al., 2012; Hardison et al., 2012, 2013). Despite the research done, the high predictability of its occurrence, and impact on local economy, surprisingly little is known about some key features of this photoautotrophic species, e.g. the modes of inorganic carbon acquisition, which can explain and predict how this species is able to thrive during dense blooms or how it will respond to enhanced CO_2 in a future ocean. Only a few studies have investigated the response of this important species to changes in CO_2 concentrations (Errera et al., 2014; Hardison et al., 2014). Briefly, Hardison et al. (2014) investigated three strains of *K. brevis* under ambient and reduced CO_2 (CCMP 2228, CCMP 2229, and SP3) and found reduced growth and enhanced brevetoxin per cellular carbon under reduced CO_2. Errera et al. (2014), using two different strains of *K. brevis* (SP1 and Wilson clone), tested low, ambient, and high CO_2 concentrations and found a substantial increase in growth with elevated CO_2 but no changes in toxin production and/or growth were detected between ambient and low CO_2. While different strains and additional parameters, such as temperature, were tested in these studies, the opposing CO_2 dependent trends in brevetoxin production and an omitted mechanistic understanding of the responses calls for additional investigation of the response including studies on key physiological processes such as photosynthesis and carbon acquisition to a range of CO_2 concentrations.

Identifying the response of underlying physiological mechanisms to changes in CO_2 concentration can highlight the limitations and trade-offs in physiological pathways, which are key for determining and predicting the competitive abilities of this species. It is the goal of this study to provide a process-level investigation to better understand the previously measured physiological responses of *K. brevis* to CO_2 levels.

Growth, elemental composition, and brevetoxin production responses to the changes in CO_2 concentrations, representative of current (400 µatm), projected future atmospheric concentrations (780 µatm), and conditions simulating dense blooms with reduced CO_2 (150 µatm) were measured. In order to understand those physiological responses, photosynthesis and photophysiology, as well as inorganic carbon acquisition mechanisms (kinetics and inorganic carbon source preferences, carbonic anhydrase activity, RubisCO saturation) were studied.

2. Materials and methods

2.1. Culture conditions

Karenia brevis (CCFWC-126), isolated from the Gulf of Mexico (Tampa area) and provided to us by the Florida Fish and Wildlife Commission, was used for the purpose of regional relevance. *K. brevis* (CCFWC-126), as opposed to strains used in previous studies (e.g. SP1, SP3, Wilson), is a fresh isolate from the Florida Shelf, an area which is continually affected by *Karenia* red tide blooms in recent years, yet, data describing the ecophysiology of the strains occurring in this region is scarce. Cultures of *K. brevis* were grown in semi-continuous batch approach at 26 °C in 1L polycarbonate bottles with a 12:12 h light:dark cycle at 100 µmol photons m^{-2} s^{-1} (GE Daylight Ecolux® T12). Light intensities were sub-saturating (Section 3.4) but chosen in order to be able to compare data with existing literature. Cells were grown in 0.2 µm filtered unbuffered modified Aquil media with f/2 vitamin recipe (Guillard and Ryther, 1962; Price et al., 1989). Modifications of the media recipe included changes in concentration of Phosphate, Zinc, Manganese, and Copper, added to final concentrations of 1.5×10^{-5} M, 1×10^{-7} M, 2×10^{-8} M, 1.0×10^{-8} M, respectively. Vanadium and Chromium were added to final concentrations of 1×10^{-8} M. No silica was added to the media. The modifications were chosen as we determined that cells grew better in this modified medium compared to standard Aquil and L1-Si recipes. In order to reach the target CO_2 concentrations and keep them stable throughout the growth of the cultures, media was vigorously pre-bubbled with air containing 150, 400, and 780 µmol CO_2 for at least 24 h before adding the cells. Once cells were added, cultures were very gently bubbled with care taken to maintain bubbling at low rates of ~4 mL min^{-1} as dinoflagellates have been found to be sensitive to fast bubbling in this experiment and others (van de Waal et al., 2014, Martin et al., 2003) while keeping the headspace of culture bottles filled with the appropriate pCO_2 air through the use of an exhaust system. Using this approach and low cell densities (maximum ~6000 cells/ml) the cells were acclimated to the respective CO_2 concentration over the duration of the exponential growth. While carbonate chemistry was not perfect and shifted slightly during cell growth, it was clearly different between the different acclimations. CO_2 concentrations were obtained by using mass flow controllers (Alicat Scientific) to mix CO_2-free air (CO2-PG80, Pure Air) with pure CO_2 (Airgas), or by using ambient room air (~400 µatm). Mid-experiment, the ambient culture was switched to 400 µatm using an additional line in the gas-mixing system. Cultures were acclimated for at least 7 generations at the respective CO_2 before being used for any experiments or before growth rates were determined (approximately 4 weeks of acclimation). Cultures were maintained in triplicate. A separate un-bubbled control culture kept at ambient pCO_2 (~400 µatm) was used to check for a mechanical bubbling effect on growth rates. Regular dilutions with pre-acclimated media rigorously bubbled with target pCO_2 for several days assured an equilibrated carbonate chemistry. Cells were able to grow exponentially up to 10 days before reaching stationary phase but, were diluted within 7 days as the carbonate chemistry started to shift (by 0.1 pH unit increase).

2.2. Carbonate chemistry

Air pCO_2 was verified using a LI-820 CO_2 analyzer (LI-COR, Lincoln, Nebraska, USA). Dissolved inorganic carbon (DIC) was measured in culture media following a modified protocol from Noguchi et al. (2013). Measured standards included water with 3.4% NaCl bubbled with CO_2-free air, freshly prepared HCO_3^- standards with known final concentrations, preacclimated culture media prior to the addition of cells, as well as culture media from the mid-exponential growth phase. For the latter, cells were removed via filtration using an inline filter and a peristaltic pump. Exact methods for DIC analysis can be found in the supplemental materials (Method S1). Carbonate chemistry in the cultures was monitored daily by measuring culture pH (Zhang and Byrne, 1996). When cultures drifted by more than 0.1 pH, cells were immediately diluted with pre-acclimated medium and were not used for experiments for several generations. Carbonate chemistry was calculated using CO_2 sys (Pierrot et al., 2011) with input parameters: Temp 26 °C, Salinity 35, PO_4^{3-} 50, Si 0, DIC (as measured), pH (as measured and converted to NBS scale). CO_2 constants K1, K2 from Mehrbach et al. (1973) refit by Dickson and Millero (1987) were chosen, KSO_4 source was by Dickson (1990), and total boron source was used as defined by Uppström (1974).

2.3. Growth, chlorophyll a, elemental composition, brevetoxin analysis, protein concentration

Specific growth was measured via cell count (using a Coulter Counter Z2 (Beckman, Indiana, USA, size detection 12 and 30 µM)) and relative chlorophyll fluorescence (Relative Fluorescence Units) (Trilogy, Turner Design, California, USA) throughout the experimental phase. Chlorophyll *a* $cell^{-1}$ (Chl *a*) was determined by filtering cells via gravity filtration onto a GF/F filter. In general, all filter samples were taken using gravity filtration to avoid breaking of the cells. Filters were stored immediately at −20 °C or −80 °C until further analysis. Chlorophyll *a* was extracted in 90% acetone for 24 h with subsequent measurement using a UV/VIS spectrophotometer (Evolution 220, ThermoFisher, Massachusetts, USA) at the wavelengths 750, 663, 645 and 630 nm (following the ESS Method 150.1) (Eq. 1):

$$Chlorophyll\ a\ (\mu g\ Chl\ a\ L^{-1}) = \frac{s \times (11.85 \cdot A_{664} - 1.54 \cdot A_{647} - 0.08 \cdot A_{630})}{V \times L} \quad (1)$$

where s = the volume (mL) of acetone used for the extraction (mL), V = the volume of water filtered (L), L = the cell path length (cm). For particulate organic carbon (POC) and nitrogen (PON) analysis, 100 mL of culture were filtered onto precombusted GF/F filters (5 h–500 °C), acidified, dried, and subsequently analyzed using a continuous flow Isotope Ratio Mass Spectrometery by the UC Davis Stable Isotope Lab. Blanks were taken for each measurement using culture media prior to the addition of cells. Brevetoxin samples were extracted following Roth et al. (2007) and measured using a brevetoxin ELISA kit which specifically measures PbTx-2 and PbTx-3 (Abraxis Inc, Warminster, PA, USA). Exact methods for brevetoxin extraction can be found in the supplemental materials (Method S2). Total cellular protein was determined using the BCA protein assay kit (Pierce, Thermo Scientific, Waltham, MA, USA).

2.4. Photophysiological parameters

Photosynthesis vs. irradiance fluorescence induction light curves (FLC) were measured using a Fast Repetition Rate Fluorometer (FRRf, FastOcean PTX, Chelsea Technologies Group) along with a FastAct Laboratory system (Chelsea Technologies). Each FLC measurement lasted 1.5 h and cultures were measured continuously over a 24 h period. Between FLCs, cultures were exchanged using the peristaltic pump controlled by the FRRf. Cells were acclimated to each light intensity for 3 min. Additional details on the FLC settings can be found in the supplemental materials (Method S3). Photophysiological data such as Fo, Fm, Fo′, Fm′, E_k (light saturation parameter), σ_{LHII} (a measure of

the functional absorption cross section of PSII), τ_{ES} (the time constant for the re-opening of a closed RCII with an empty Q_b site), and NPQ (a measure of nonphotochemical quenching) as estimated as the Stern-Volmer coefficient of quenching, defined as NPQ = (Fm - Fm′) / Fm′ were obtained. Derivation of these photochemical variables can be found in Oxborough et al. (2012). To calculate gross primary production (GPP) from FRRf data (GPP_{FRRf}), we used data from the 121 μmol photons m^{-2} s^{-1} (closest light intensity to acclimation light measured in the FRRf) and the following equation from Lawrenz et al. (2013) to calculate electron transport rates (ETR) in units of mol electron^{-} (mg Chl *a*)$^{-1}$ h^{-1} (Eq. (2)):

$$ETR = E \times \sigma'_{LHII} \times n_{PSII} \times (F'_q/F'_v) \times \Phi_{RC} \times 2.43 \times 10^{-5} \quad (2)$$

where E is light intensity, σ_{LHII}' is the functional absorption cross section of PSII in the light (Å^2 quanta^{-1}), n_{PSII} is a conversion factor for reaction centers to chl *a* (mol reaction centers mol Chl a^{-1}) with a value of 0.002 based on values obtained from eukaryotic phytoplankton (Kolber and Falkowski, 1993; Raateoja et al., 2004), (F_q'/F_v') is the light adapted quantum yield, Φ_{RC} is the electron yield from each RCII charge separation equaling 1 based on Lawrenz et al. (2013), and 2.43 × 10^{-5} is used as a unit conversion factor (Lawrenz et al., 2013). To further convert ETR into GPP (mol C mg Chl a^{-1} h^{-1}), we used the conversation factor $\Phi_{e,C}$ (mol electrons mol CO_2^{-1}) of 10 (Lawrenz et al., 2013) (Eq. (3)):

$$GPP_{FRRf} = ETR \times \Phi_{e,C} \quad (3)$$

To calculate net primary production from the FRRf (NPP_{FRRf}), we used the GPP_{FRRf} data and the carbon-based GPP/Respiration (GP_C/R) ratio data (Eq. (4)):

$$NPP_{FRRf} = GPP_{FRRf} - (GPP_{FRRf} \times R/GPP_C) \quad (4)$$

2.5. Photosynthetic oxygen evolution

Photosynthetic oxygen evolution was measured using a FirestingO2 optical oxygen meter (Pyro Science, Germany). Cultures in exponential growth phase were concentrated using gravity filtration over a 10.0 μm PTFE filter and subsequently resuspended into the measuring bottles using fresh CO_2 equilibrated media. Care was taken to not let cells dry out (a thin film of media covered the cells at any point) and F_v/F_m measurements prior to and after filtration revealed no significant change (Data not shown). Cells were subsequently placed into gastight oxygen optode bottles (respiration bottles, Pyro Science, Germany), kept at 26 °C and illuminated by LED lights (Bright White LED Strip Lights, Cool White) at 100 μmol photons m^{-2} s^{-1}. Cultures were stirred gently to ensure homogenous gas distribution as well as to avoid any potential cell clumping or settling. Measurements were started in the dark period and lasted 24 h. Light-dark timing was set to the same cycle as the cells in the different pCO_2 acclimations were exposed to. Additionally, three 30 min dark periods were set to quantify dark respiration during the light phase. Light-dependent respiration (e.g. photorespiration, chlororespiration) was not analyzed. Data was fit using linear regressions in ~30 min increments throughout the light period to determine high resolution net primary productivity rates (NPP_O) and throughout the dark periods to determine dark respiration (R) rates. A sample of the cell concentrate was taken before and after the measurements and the average cell number and/or chl *a* concentration was used to normalize rates of O_2 production/respiration. Dark respiration ($R_{O\text{-}light}$) during the light phase was determined by linear extrapolation of the three oxygen consumption measurements during the light phase. Oxygen-based gross primary productivity (GPP_O) was calculated as follows (Eq. (5)):

$$GPP_O = NPP_{O-light} - R_{O-light} \quad (5)$$

where $NPP_{O\text{-}light}$ equals the rate of O_2 evolution in the light.

In order to calculate gross productivity on a per carbon basis (GPP_C), we used NPP_O and applied a photosynthetic quotient of 1.4 (for nitrate usage) as well as a respiratory quotient of 1 (Wiliams and Robertson, 1991) (Eq. (6)):

$$GPP_C = NPP_O/1.4 - R_{O-night} \quad (6)$$

As a second estimate of net carbon production, the calculated specific growth rate μ (d^{-1}) was multiplied by C $cell^{-1}$ (Eq. (7)):

$$NPP_\mu = C\ cell^{-1} \times \mu \quad (7)$$

Theoretical calculation of carbon fixation, based on growth rate and estimated cellular RubisCO concentration were conducted as shown in Losh et al. (2013) using the growth rates, C $cell^{-1}$ and protein $cell^{-1}$ data (Table S1).

2.6. Carbon acquisition measurements

Cultures were concentrated using the same gravity filtration method described in photosynthetic oxygen evolution rate experiments. Cells were washed and resuspended in CO_2-free Aquil media buffered with 50 mM BICINE adjusted to the pH of growth conditions. Care was taken to not introduce CO_2 through bubble injection and cells were illuminated for up to 20 min to reduce potential introduced CO_2.

The ^{14}C disequilibrium method was used to determine the steady state fraction of $H^{14}CO_3^-$ and $^{14}CO_2$ uptake in the cells after the relatively high pH measurement media (7.9–8.3) is spiked with a relatively low pH (5.75–6.7) ^{14}C solution (Espie and Colman, 1986; Rost et al., 2007; Kottmeier et al., 2014). Data analysis was done using Graphpad Prism 7 (GraphPad Software, La Jolla California USA).

Carbon uptake kinetics were determined using the ^{14}C fixation method described by Tortell et al. (2010) where cells were incubated with $H^{14}CO_3^-$ for 10 min over a range of inorganic carbon concentrations (16, 40, 116, 166, 333, 662, 1316, 2042, 3196, and 3881 μM DIC). Cells were prepared as described above. For both disequilibrium and kinetics measurements, reactions were stopped by transferring 600 μl of culture into 600 μl of 6 M HCl with a subsequent degassing time of 24 h. 6 mL of scintillation cocktail was added, and samples were counted in a Liquid Scintillation Counter (PerkinElmer TriCarb 5110 TR) to obtain disintegrations per minute. Curves were fit using Graphpad Prism 7 (GraphPad Software, La Jolla California USA) with a Michaelis-Menton equation (Eq. (8)):

$$V = V_{max}[S]/K_{1/2} + [S] \quad (10)$$

where V is reaction rate, V_{max} is the maximum reaction rate, [S] is the substrate concentration, and $K_{1/2}$ is the half saturation concentration of the cell to DIC.

Extracellular carbonic anhydrase (eCA) activity was measured according to Rost et al. (2007), based on Silverman (1982) with slight modifications. Cultures were concentrated by gravity filtration and growth media was exchanged stepwise with CO_2-free Aquil media buffered with 50 mM BICINE adjusted to match pH of growth conditions as close as possible (7.9, 8.1, or 8.3). Analysis of cell size distribution and F_v/F_m prior to and after concentration showed no significant differences (Data not shown) and ensured the health and intactness of the cultures. Cells were further concentrated using gentle centrifugation at 250 rpm for 1 min before being measured with a membrane-inlet mass spectrometer (MIMS, Pfeiffer, PrismaPlus QMC220, Germany) with a custom-made cuvette system (10 mL volume). CA activity was determined by adding HCO_3^- labeled with ^{13}C and ^{18}O to the media and the uncatalyzed rate of ^{18}O loss, which is caused by the hydration and dehydration steps of CO_2 and HCO_3^- in water was recorded. This was measured for 5 min after reaching equilibrium. Subsequently, 150–250 μl of the concentrated cells suspension was added to the media. The rate of ^{18}O depletion with cells (S2) was compared to the uncatalyzed rate (S1). Rates were normalized to chl *a* (Eq. (9)):

Table 1
Carbonate chemistry measured and calculated in the experiment. Data are given for carbonate chemistry measured prior to the addition of cells, as well as during mid exponential growth phase.

Measured pCO_2 (µatm) in Gas Line		150	435	780
Abiotic Carbonate Chemistry	DIC (µM)	1679 ± 2	2008	2089 ± 1
	pH media (NBS)	8.51 ± 0.04	8.12 ± 0.02	7.89 ± 0.01
	Calculated pCO_2 (µatm)	118.9 ± 0.1	446.6 ± 31.0	812.7 ± 0.5
	Calculated TA (µmol/kg seawater)	2320 ± 3	2348 ± 18	2309 ± 1
	CO_2 (µmol/kg seawater)	3.3 ± 0.0	12.3 ± 0.9	22.4 ± 0.0
	HCO_3^- (µmol/kg seawater)	1286 ± 2	1793 ± 11	1937 ± 1
Carbonate Chemistry after cells grown to mid exponential phase	DIC (µM)	1714 ± 4	1982 ± 26	2103 ± 4.
	pH media (NBS)	8.63 ± 0.05	8.22 ± 0.03	7.95 ± 0.04
	Calculated pCO_2 (µatm)	102.9 ± 16.8	355.6 ± 30.4	753.4 ± 78.8
	Calculated TA (µmol/kg seawater)	2428 ± 64	2376 ± 14	2342 ± 19
	CO_2 (µmol/kg seawater)	2.8 ± 0.5	9.8 ± 0.8	20.8 ± 2.2
	HCO_3^- (µmol/kg seawater)	1268 ± 43	1734 ± 35	1941 ± 13

$$U = S2/(S1 - 1) \quad (9)$$

where U represents the enhancement factor, expressed as an x-fold increase in the interconversion rate between CO_2 and HCO_3^-.

3. Results

3.1. Carbonate chemistry

The carbonate chemistry in this experiment is reported in Table 1. The measured values of DIC and pH between the different pCO_2 acclimations and calculated dissolved CO_2 concentration proved to be significantly different between all pCO_2 acclimations. Calculated total alkalinity (calculated from DIC and pH) showed relative constant values (2309–2347 µmol/kg seawater in the pre-acclimated media) and slightly drifted values (2341–2428 µmol/kg seawater) in the media which contained cultures. Concentrations of calculated pCO_2 and measured pCO_2 (based on calculation in CO2sys using DIC and pH) were relatively similar within each of the different pCO_2 acclimations with the largest difference seen in the 150 µatm culture between pre-acclimated media and media in which cells were grown (Table 1). Carbonate chemistry compared between pre-acclimated media and the media measured from mid exponentially grown cells (Table 1) showed that measured DIC was stable within the methodological accuracy. The drift in pH during cell growth nonetheless resulted in a drift in the target pCO_2 and TA (Table 1) indicating small drifts of the carbonate chemistry during cell growth. Dissolved CO_2 concentrations of the medium in which cultures grew to mid exponential phase were calculated to be 2.8 ± 0.5, 9.8 ± 0.8, 20.8 ± 2.2 µmol/kg seawater and HCO_3^- concentrations were calculated to be 1268 ± 43, 1734 ± 35, 1941 ± 13 µmol/kg seawater in the 150, 400, and 780 pCO_2 acclimations, respectively.

3.2. Growth, chlorophyll a, elemental composition, brevetoxin analysis, protein concentration

Growth rates for the 150, 400, and 780 µatm cultures as well as the control were: 0.21 ± 0.06 d^{-1}, 0.22 ± 0.06 d^{-1}, 0.20 ± 0.06 d^{-1}, and 0.24 ± 0.05 d^{-1}, respectively, and the bubbled acclimations were not statistically different (One-way ANOVA, $p > 0.05$, $df = 417$) (Fig. 1, Table 2). Additionally, no difference in growth was detected between the control (un-bubbled – open to atmosphere) and the 400 µatm bubbled culture (One-way ANVOA, $p = 0.0786$, $df = 417$). Average cell size for *K. brevis* also did not change across pCO_2 concentrations with average cell diameters of 22.0 ± 0.4, 22.1 ± 1 and 22.0 ± 0.3 µm for the three pCO_2 acclimations, respectively. Chlorophyll *a* $cell^{-1}$ showed a similar response with values for the three acclimations of 13.63 ± 1.26, 14.20 ± 0.57, and 15.07 ± 0.13 pg Chl *a* $cell^{-1}$ for the 150, 400, and 780 µatm cultures, respectively

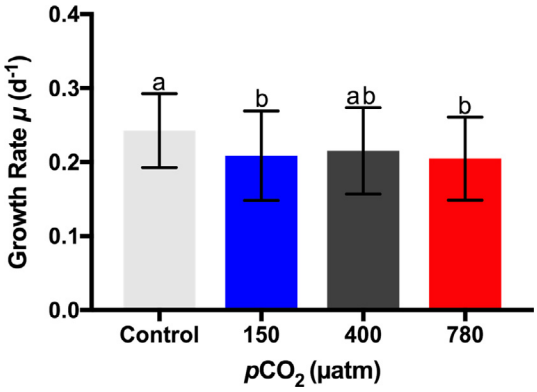

Fig. 1. Growth rates of *K. brevis* based on cell count in the different pCO_2 acclimations as well as the unbubbled control. Data shown are mean values ($n > 20$, ± SD). Statistical differences and groupings determined via ANOVA and Tukey's HSD indicated using letters (p-values < 0.05).

(Table 2). Cells/Relative Fluorescence Units ratios stayed constant (5.62 ± 0.75) throughout the exponential growth phase (Data not shown). Quotas for cellular C were 0.66 ± 0.20, 0.50 ± 0.06, and 0.51 ± 0.06 ng carbon $cell^{-1}$ and cellular N average values were 0.12 ± 0.04, 0.09 ± 0.01, and 0.09 ± 0.01 ng nitrogen $cell^{-1}$ for the 150, 400, and 780 µatm cultures, respectively (Table 2). The C/N ratio (mol:mol) was calculated as 6.57 ± 0.13, 6.83 ± 0.27, and 6.53 ± 0.22 for the 150, 400, and 780 µatm cultures, respectively (Table 2). No significant differences (one-way ANOVA) between Chl *a* $cell^{-1}$, C $cell^{-1}$, and N $cell^{-1}$ values for the different pCO_2 acclimations. The larger standard error in C $cell^{-1}$ and N $cell^{-1}$ value in the 150 µatm cultures indicates a measurement error, likely an underestimation in cell counts in two of the replicate cultures of this acclimation from this day. Brevetoxin values (PbTx-2 and PbTx-3) in pg $cell^{-1}$ were 3.43 ± 0.89, 3.91 ± 0.66, and 4.69 ± 0.37 for the 150, 400, and 780 µatm cultures, respectively (Fig. 2, Table 2) with no significant differences (one-way ANOVA). Additionally, protein $cell^{-1}$ in ng for the 150, 400, and 780 µatm cultures were 0.45 ± 0.02, 0.40 ± 0.05, and 0.43 ± 0.07, respectively (Table 2, no significant differences (one-way ANOVA)). Protein per C was calculated from Protein $cell^{-1}$ and C $cell^{-1}$ and found to be 34%, 40%, and 42% for the 150, 400, and 780 µatm cultures, respectively.

3.3. Photophysiology

No pCO_2 effects were seen on the dark adapted F_v/F_m, or in the values for E_K (light saturation point, data not shown), σ_{LHII} (functional absorption cross section of PSII, data not shown) and GPP_{FRRf} (gross productivity as analyzed via FRRf as calculated in Eqs. (6) and (7) at

Table 2
Average values for growth rate, cellular Chl a, POC, PON, C/N ratios, brevetoxin, and protein content for *K. brevis* cells under different pCO_2 treatments. Values given represent mean ± SD [$] Rates are averaged for each biological replicate. SD represents error between biological replicates. [^] Chl a, POC and PON, brevetoxin and protein per cell were taken during the middle of one exponential growth phase.

pCO_2 (µatm)	Growth rate µ (d^{-1})[$]	Chl a (pg $cell^{-1}$)[^]	POC (ng $cell^{-1}$)[^]	PON (ng $cell^{-1}$)[^]	C:N (mol:mol)[^]	Brevetoxin (pg $cell^{-1}$)[^]	Protein (ng $cell^{-1}$)[^]
150	0.209 ± 0.06	13.63 ± 1.26	0.66 ± 0.20	0.12 ± 0.04	6.57 ± 0.13	3.43 ± 0.89	0.45 ± 0.02
400	0.215 ± 0.06	14.20 ± 0.57	0.50 ± 0.06	0.09 ± 0.01	6.83 ± 0.27	3.91 ± 0.66	0.40 ± 0.05
780	0.205 ± 0.06	15.07 ± 0.13	0.51 ± 0.06	0.09 ± 0.01	6.53 ± 0.22	4.69 ± 0.37	0.43 ± 0.07

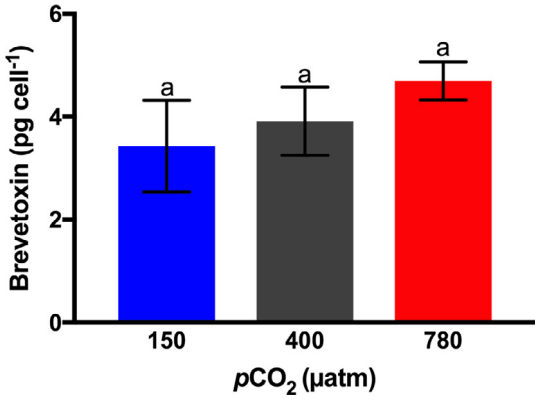

Fig. 2. Brevetoxin (pg $cell^{-1}$) for *K. brevis* in the different pCO_2 treatments. Data shown are mean values (n > 3, ± SD). Statistical differences and groupings determined via ANOVA and Tukey's HSD indicated using letters (p-values > 0.05).

121 µmol photons m^{-2} s^{-1}) for the *K. brevis* strain used in this study (Fig. 3). E_K values averaged over the light period were 483 ± 23, 489 ± 38, and 513 ± 11 µmol photons m^{-2} s^{-1} for the 150, 400, and 780 µatm acclimations, respectively. Average values of σ_{LHII} measured over the light period were 4.25 ± 0.10, 3.99 ± 0.11, and 4.10 ± 0.17 nm^2 $PSII^{-1}$ for the 150, 400, and 780 µatm acclimations, respectively. A pCO_2 effect on nonphotochemical quenching (NPQ) as well as τ_{ES} (time constant for the re-opening of a closed RCII with an empty Q_b site) was apparent for some duration of the diurnal cycle (Fig. 3C and D). During the first three quarters of the light period (6 am until 3 pm) the 780 µatm cultures had both higher NPQ and τ_{ES} values compared to the 150 and 400 µatm cultures. Additionally, during these times, a consistently higher NPQ was observed for the 780 µatm cultures under all light intensities measured (Fig. 4A and B). NPQ relaxed to values similar to the 150 and 400 µatm acclimation after 3 pm (Fig. 4C).

F_v/F_m values showed a pronounced diurnal cycle, increasing slightly from the onset of light until noon and decreasing towards the end of the light period (Fig. 3A). GPP_{FRRf} as calculated according to Eqs. (2), (3), and (4) showed a slight increasing trend until midday and a subsequent slight decrease until the end of the light period (Fig. 3B). Calculated GPP_{FRRf} from 12 pm FLCs at 121 µmol photons m^{-2} s^{-1} (the light intensity measured in the FRRf closest to acclimation light) yielded rates of 111 ± 3, 102 ± 3, and 107 ± 7 µmol C mg Chl a^{-1} h^{-1} for the 150, 400, and 780 µatm acclimations, respectively.

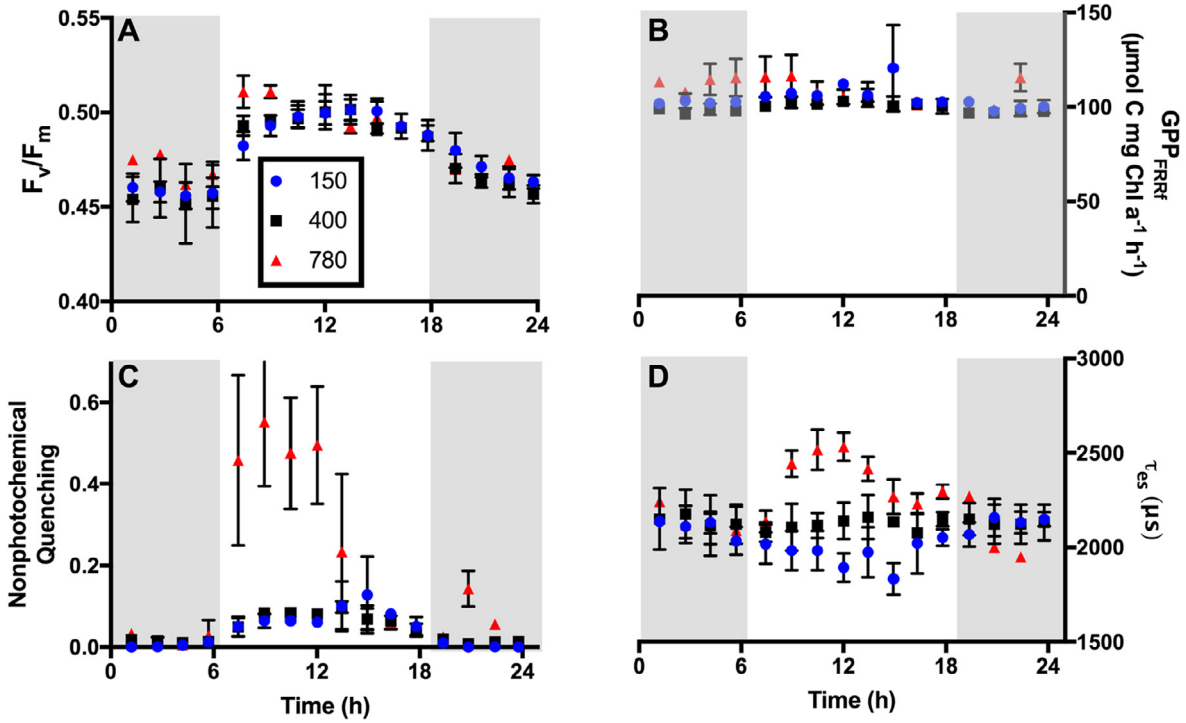

Fig. 3. Photophysiology of *K. brevis*; Dark shaded areas indicate the night time. (A) Diurnal trends of F_v/F_m values between the different pCO_2 acclimations. Please note the y-axis magnification. (B) GPP_{FRRf} values -data during dark hours indicate photosynthetic potential. (C) Nonphotochemical quenching (NPQ) for the different pCO_2 acclimations. (D) τ_{ES} for the different pCO_2 acclimations. Data shown are mean values (n ≥ 1, ± SD). Circles represent 150 µatm acclimation, Squares represent 400 µatm acclimation, and Triangles represent 780 µatm acclimation.

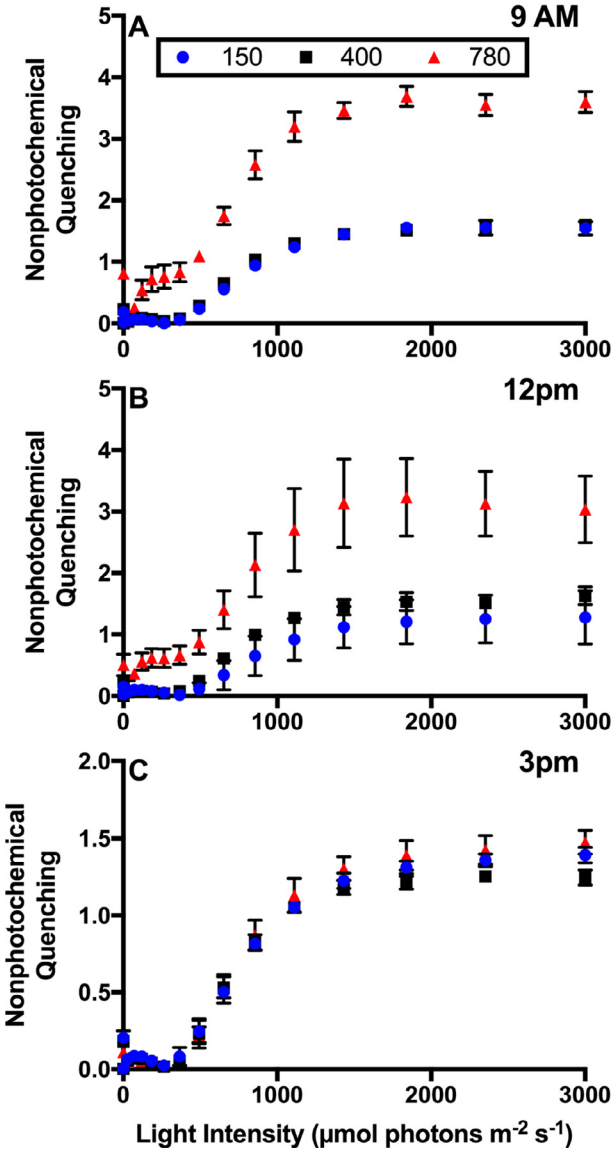

Fig. 4. Nonphotochemical quenching (NPQ) at (A) 9AM, (B) 12PM, (C) 3PM over the FLC (full light curve). Data shown are mean values (n ≥ 3, ± SD). Circles represent 150 µatm acclimation, Squares represent 400 µatm acclimation, and Triangles represent 780 µatm acclimation.

3.4. Photosynthetic oxygen evolution

Net photosynthesis in *K. brevis* was largely unaffected by the different pCO_2 treatments averaging 56 ± 6, 67 ± 6, and 60 ± 5 µmol O_2 Chl a^{-1} h^{-1} over the light period for the 150, 400, and 780 µatm cultures respectively. Average photosynthetic rates during the light period are shown in Fig. 5 and Table 3. Values of photosynthesis normalized per cell are given in the supplemental materials (Table S2). The measured rates of dark respiration averaged 37 ± 3, 26 ± 2, and 26 ± 2 µmol O_2 Chl a^{-1} h^{-1} for the 150, 400, and 780 µatm cultures respectively and accounted for approximately 40–44% of the calculated gross photosynthesis (Fig. 5, Table 3). In all three pCO_2 treatments, photosynthetic rates decreased at the end of the light period while respiration rates increased over the light period (Data not shown) and decreased during the night. In the 150 µatm cultures, night time respiration rates were significantly higher compared to the 400 and 780 µatm cultures (One-way ANOVA, $p < 0.0001$, df = 71). These diurnal trends in photosynthesis, respiration, and photophysiology (Section 3.3) indicate that *K. brevis* expresses a pronounced diurnal cycle, even

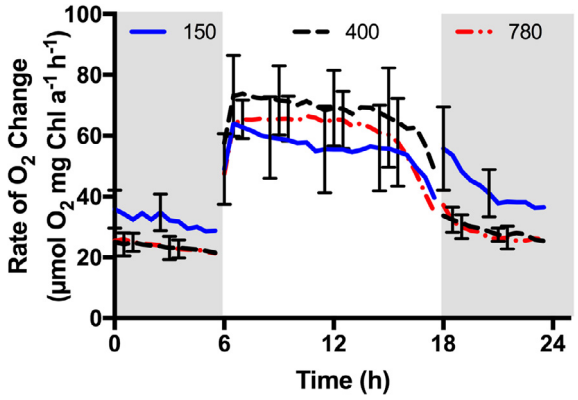

Fig. 5. Net O_2 evolution rates of *K. brevis* in different pCO_2 acclimations measured continuously throughout a 24-hour period. Non-shaded areas indicate periods of light and data shown is net primary productivity (NPP_O). Shaded areas indicate dark periods (night) and lines in these areas are representative of respiration rate (R). Respiration rates are shown as positive values for clarity. Data shown are mean values (n > 3, ± SD). Error bars are staggered by 30 min. for clarification, with the left most error bar representing 150 µatm, middle error bar representing 400 µatm, and right most error bar representing 780 µatm.

Table 3
Measured Net and Gross Primary Productivity and Respiration rates from 24 h experiments. Average rates over the light phase (NPP, GPPP) or the dark period (R_O, R_C) are shown. Values given represent mean ± SD of n = 3. Units are as follows: NPP_O, GPP_O and R_O: (µmol O_2 mg Chl a^{-1} h^{-1}); NPP_C: GPP_C: R_C (µmol C mg Chl a^{-1} h^{-1}).

pCO_2 (µatm)	NPP_O	GPP_O	R_O	NPP_C	GPP_C	R_C
150	56 ± 6	99 ± 12	37 ± 3	40 ± 5	83 ± 10	37 ± 3
400	67 ± 6	112 ± 8	26 ± 2	48 ± 5	93 ± 7	26 ± 2
780	60 ± 5	104 ± 6	26 ± 2	43 ± 3	87 ± 5	26 ± 2

in laboratory cultures under constant 12-hour light exposure.

3.5. Carbon acquisition

3.5.1. Kinetics

Values for $K_{1/2}$ (CO_2) were 1.36 ± 0.24, 1.64 ± 0.27, and 3.36 ± 0.49 µM for the 150, 400, and 780 µatm cultures, respectively (Fig. 6A). The 780 µatm cultures showed a significantly higher $K_{1/2}$ (CO_2) (One-way ANOVA, $p = 0.0008$, df = 8) compared to 150 and 400 µatm cultures. The respective $K_{1/2}$ (DIC) were 333.1 ± 58.1, 247.0 ± 40.3, and 294.6 ± 42.6 µM showing no statistically significant differences (One-way ANOVA, $p = 0.94$, df = 8). It should be noted that the measurements were conducted in pH adjusted media (close to the respective acclimation pHs of 7.9, 8.1, 8.3, respectively) and that dissolved CO_2, HCO_3^- and CO_3^{2-} concentration ratios varied in the respective assays.

3.5.2. C-source preference

Higher dissolved CO_2 in the media resulted in a significant increase in CO_2 utilization with 14% ± 1%, 26% ± 5%, 56% ± 8% CO_2 uptake for the 150, 400, and 780 µatm cultures, respectively, (One-way ANOVA, $p = 0.0002$, df = 8) (Fig. 6B). Hence active HCO_3^- pumping to supply RubisCO with inorganic carbon was reduced under high pCO_2.

3.5.3. External CA activity

Each pCO_2 acclimation showed activity of eCA. Values for the 150, 400, and 780 µatm cultures were 6.69 ± 0.71, 5.43 ± 0.75, and 5.12 ± 0.67 U (µg Chl a^{-1}). Notably, the 150 µatm cultures had

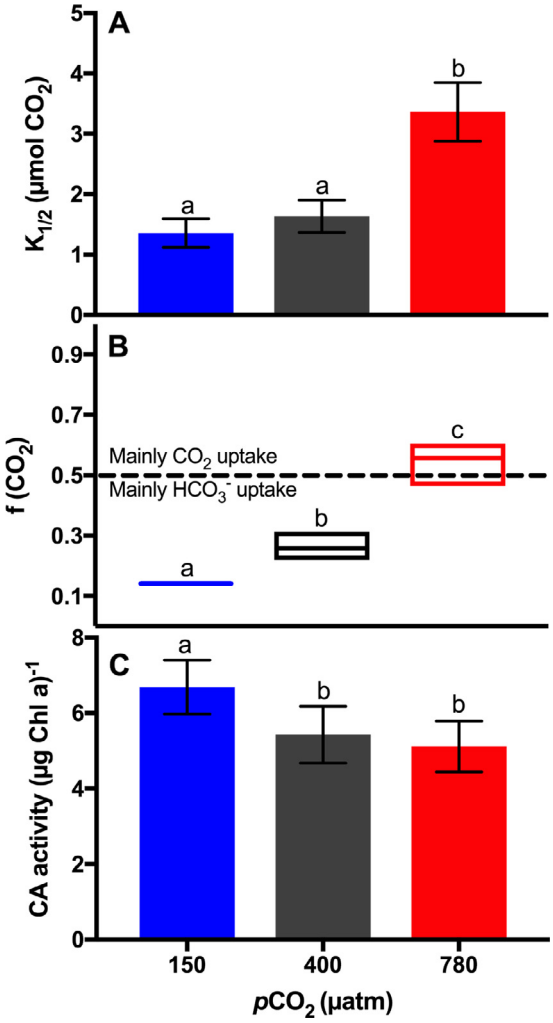

Fig. 6. CCM parameters measured in the experiment. (A) Half saturation constants for CO_2, (B) Fraction CO_2 to HCO_3^- utilization. (C) eCA activity. Data shown are mean values (n ≥ 3, ± SD). Statistical differences and groupings determined via ANOVA and Tukey's HSD indicated using letters (p-values < 0.05).

significantly higher eCA activity (One-way ANOVA, $p = 0.0016$, $df = 2$) (Fig. 6C).

4. Discussion

This study aimed to understand underlying mechanisms of a potential CO_2 sensitivity in the dinoflagellate *Karenia brevis* (Errera et al., 2014; Hardison et al., 2014). Despite partially contradicting each other in their growth and brevetoxin production responses under low CO_2 concentrations, both of those studies indicated that CO_2 can affect the cellular physiology of *K. brevis*, leading to altered growth and changes in production of brevetoxin. As suggested by Errera et al. (2014), underlying processes such as insufficient inorganic carbon supply under "low" CO_2 (55–245 µatm) to support the C-fixing enzyme RubisCO could have resulted in the reduced growth under the low and ambient CO_2 concentrations measured in their study. Hardison et al. (2014) hypothesized, however, that *K. brevis* must have a relatively efficient CCM. In Hardison et al. (2014), low pCO_2 was also found to induce cellular brevetoxin production while in Errera et al. (2014) toxin production did not change on the per cell level. Here we analyzed similar cellular responses, and additionally quantified photosynthesis and modes of carbon acquisition (the CCM) under low, ambient, and high CO_2 concentrations. Furthermore, we characterized diurnal processes of photosynthesis and photophysiology, e.g. light quenching mechanisms, which have been suggested to be affected by brevetoxin (Cassell et al., 2015).

One of the challenges of growing non-armored dinoflagellates such as *K. brevis* under different CO_2 concentrations is that mechanical shear stress, as implemented by bubbling, can harm the integrity of the cells (van de Waal et al., 2014, Martin et al., 2003). We used an undisturbed culture (acclimated to atmospheric pCO_2) as a control to identify potential physical shear stress on growth, morphology and photosynthetic yield response. The collected data indicate that the gentle bubbling performed to keep carbonate chemistry stable did not significantly alter rates of growth (comparing the control and the 400 µatm acclimation culture – Fig. 1) nor did it change photosynthetic yield or cell size (Data not shown).

Growth, cellular C and N quotas, and cellular chl *a* did not show a distinct CO_2 response in this study and are in contrast to the two studies previously published on the effects of CO_2 on *K. brevis* (Table 2, Figs. 1 and 2) (Errera et al., 2014; Hardison et al., 2014). While the measured average growth rates (0.2–0.24 d^{-1}) were slightly lower compared to Errera et al. (2014) (growth rates of ~0.30 d^{-1}) and Hardison et al. (2014) (growth rates of 0.30–0.55 d^{-1}), these differences might be a strain specific trait response. However, other potential triggers such as differences in acclimation methods (carbonate chemistry modification methodology, growth medium) cannot be ruled out.

Brevetoxin production (PbTx-2 and PbTx-3) of our strain of *K. brevis* (CCFWC-126) showed an increasing trend with increasing CO_2 (Table 2, Fig. 2), but, this trend is not statistically significant in the measured CO_2 range. Results from this study agree with Errera et al. (2014) where no significant CO_2 effect on cellular brevetoxin concentration was found. In contrast, Hardison et al. (2014) found increasing cellular brevetoxin in *K. brevis* grown under low pCO_2. It should be noted that the CO_2 concentration in the low pCO_2 acclimation in Hardison et al. (2014) was much lower than in this study. While the ELISA assay used in this study fully binds to PbTx-2 and PbTx-3, it does not significantly react with PbTx-1. However, the contributions of the different brevetoxins (PbTx-1, 2, and 3) and total brevetoxin shows that PbTx-1 only accounted for 3.69 ± 2.64% of total brevetoxin (Pierce and Henry, 2008) in *K brevis* found along the West Florida Shelf in the GoM. Therefore, despite not fully measuring all brevetoxin molecular structures, the data shown here should be representative of the majority of brevetoxin content in *K. brevis*. In general, responses in toxin production in dinoflagellates (and diatoms) to changes in CO_2 are diverse (e.g. Fu et al., 2010; Sun et al., 2011; Tatters et al., 2012, 2013; Hattenrath-Lehmann et al., 2015). If the response to CO_2 is indeed strain specific, it would indicate that strains which respond positively in growth to increasing CO_2 could increase in abundance in a future ocean. For toxin producing species, this could affect ecology as well as human health and economy if toxin production itself is additionally stimulated.

While much of the brevetoxin synthesis pathway is unknown, it requires inorganic carbon and cellular energy (Calabro et al., 2014). Brevetoxin is thought to be synthesized from acetyl CoA and additional acetate groups (Van Dolah et al., 2009) coupled to glycolysis and the tricarboxylic acid cycle, which are clearly linked to cellular carbon metabolism and cellular energy and reductants is needed to fuel these processes. As shown in Hardison et al. (2012, 2013, 2014), brevetoxin content as a percent of cellular carbon is approximately 0.8–2.1% for nutrient replete *K. brevis* cultures. Brevetoxin content as a percent of cellular C values measured here ranged from 0.32 to 0.62%. As brevetoxin is only a small percentage of cellular carbon, and CCMs and glycolysis are not directly linked, the response is likely not directly triggered by CO_2 availability. Nonetheless, it cannot be ruled out that a potential reallocation of cellular energy and reductants toward brevetoxin production could result in changes in cellular brevetoxin content.

The CO_2 insensitivity of *K. brevis* strain CCFWC-126 indicates that this strain is capable of maintaining growth and cellular composition under a wide range of CO_2 concentrations, indicative of an efficient

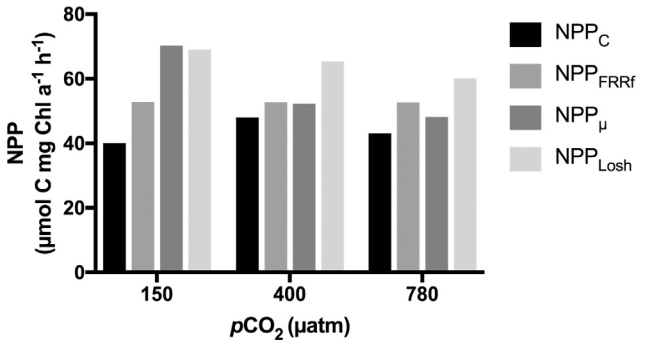

Fig. 7. Net primary productivity measured and calculated using different parameterization. NPP_C from oxygen evolution converted to C-fixation; NPP_{FRRf} using FLC data from 12 pm at 121 µmol photons $m^{-2} s^{-1}$ and equations from Lawrenz et al. (2013); $NPP_µ$ calculated using growth rate (µ (d^{-1})) and POC $cell^{-1}$; NPP_{Losh} calculated based on Losh et al. (2013) using growth rate (µ (d^{-1})), R/GPP ratio, and protein $cell^{-1}$ data.

CCM or a RubisCO half saturation concentration less that of the ambient dissolved CO_2 in the seawater. Rates of net and gross photosynthesis from the different pCO_2 acclimations support both hypotheses (Fig. 5, Table 3). NPP_{FRRf} estimates showed strong agreement with the NPP_C estimates obtained from oxygen evolution data (Fig. 7), further supporting the idea that the range of CO_2 tested in the acclimations here is not directly influencing photosynthesis. While other studies found enhanced respiration under elevated pCO_2 (Wu et al., 2010; Gao et al., 2012; Yang and Gao, 2012; Eberlein et al., 2014), this study found an increase in night-time respiration under low pCO_2, potentially alleviating external pH stress (Fig. 5, Table 3) (Hansen, 2002). A diurnal cycle, similar to that observed in this study, has been seen in gene expression of photosynthetically relevant genes of *K. brevis* (Van Dolah et al., 2007) and in photosynthesis and respiration measurements of *K. brevis* in the field (Hitchcock et al., 2014). These diurnal cycles are seen in many organisms and, despite numerous ecophysiological implications, have some important implications for experimental approaches. For instance, it is important to sample at similar times of the day because cellular composition (such as C:N ratio, Chl *a* $cell^{-1}$ or even brevetoxin $cell^{-1}$) could be affected by this cycle.

In order to gain a process-based understanding of responses of growth and photosynthesis, photophysiological data over a 24 h cycle was analyzed. The measured diurnal pattern in dark adapted F_v/F_m (Fig. 3A) indicate a diurnal regulation in photosynthetic machinery. In this study, light was sub-saturating (as indicated in the higher E_K values compared to acclimation light), hence no photostress was initiated which would otherwise lead to a reduced F_v/F_m. The enhanced NPQ and τ_{ES} values in the 780 µatm acclimation (Figs. 3C, D and 4) indicate that the electron transport chain including the plastoquinone pool are more reduced and that the cells experience an elevated proton gradient across the thylakoid membrane, especially earlier in the day. We conclude that cells grown under enhanced CO_2 have a lower demand for ATP during the earlier hours of the photoperiod due to the reduced active transport of HCO_3^- which requires approximately 1 mol ATP for every 2 mol HCO_3^- transported over the membrane (Hopkinson et al., 2011; Kranz et al., 2015; Eichner et al., 2014). The reduction in energetic cost of inorganic carbon transport can cause the increase in the transmembrane proton gradient, especially when oxygenic photosynthesis is constant. The relaxation of NPQ seen in the 780 µatm cultures at the end of the photoperiod (Fig. 3C), which likely reflects a relaxation of the transmembrane proton gradient, is probably caused by an increase in oxidative pentose phosphate pathway, as indicated by higher respiration rates during this time (Data not shown), where ATP is utilized to generate glucose-6-phosphate.

An interesting, yet extremely hypothetical, explanation of some of the measured NPQ data could be that brevetoxin interacts with the light harvesting complex in PSII, facilitating NPQ, as suggested by recent studies (Cassell et al., 2015; Chen et al., 2018). However, since we did not find any significant changes in brevetoxin content, this will likely not explain the enhanced NPQ in the 780 µatm acclimation.

In conclusion, despite small changes in photophysiology, net photosynthesis of *K. brevis* is not affected by CO_2. Comparisons of growth and productivity (NPP_{FRRf}, $NPP_µ$, NPP_C, and calculated NPP_{Losh}) show similar overall rates and patterns and support the observed CO_2 insensitivity of *K. brevis* (Fig. 7, Tables S1–S4). Despite the large amount of assumptions included in some of those estimates, a very good agreement was observed.

K. brevis has shown a close phylogenetic relationship to the haptophyte *Pavlova lutheri* via analysis of both photosystem I and RubisCO genes (Yoon et al., 2005, 2002). *P. lutheri's* RubisCO K_m value was measured to be 17.6 µM (Heureux et al., 2017), which is one of the most efficient RubisCO carboxylation kinetics measured in phytoplankton. Despite the supposedly efficient RubisCO, *K. brevis* contains and maintains pyrenoids, one of the components of a CCM (Giordano et al., 2005; Monroe et al., 2010). Consequently, it should be asked if the cells require additional aspects of the CCM (such as Cas or HCO_3^- uptake transporters), a supposedly expensive mechanism, to acquire sufficient inorganic carbon for growth and reproduction.

We therefore calculated the theoretical carbon demand, C-fixation potential, and growth without and with a potential CCM. Calculations assuming C-uptake in *K. brevis* lacking a CCM (relying on diffusive CO_2 uptake only) and assuming a similar K_m value of RubisCO as found in *P. lutheri* (K_m = 17.6 µM) yield only a 16% RubisCO saturation under 150 µatm and a 56% CO_2 saturation of RubisCO under 780 µatm (assuming a constant CO_2 concentration at RubisCO similar to the equilibrated medium). RubisCO saturation is likely lower than those assumed above as internal CO_2 has to be slightly lower compared to the external concentration in order for diffusive CO_2 uptake to happen (Hopkinson et al., 2011). Since sufficient and similar growth under "non-CCM" conditions in the CO_2 concentration range tested is unlikely, we used our data on cellular composition and photosynthetic rates following Losh et al. (2013) (Tables S3 and S4) with modifications based on measured respiration rates (Tables S3 and S4) to calculate the theoretical growth rates of *K. brevis*. Assuming ~ 85% CO_2 saturation of RubisCO (Fig. 6), theoretical specific growth rates of around 0.18 d^{-1} for 150 µatm, 0.28 d^{-1} for 400 µatm, and 0.26 d^{-1} for 780 µatm were calculated. Those rates match the growth rates measured in this study fairly well (Fig. 1, Tables S3 and S4). Based on those calculations and assumptions, it is implicit that *K. brevis* must possess an CCM to saturate RubisCO and obtain the constant growth and productivity rates observed under the CO_2 concentrations tested here.

In general, any process enhancing the supply of CO_2 to RubisCO is considered a part of the CCM. The CCM in *K. brevis* was found to rely on CO_2 as well as HCO_3^- uptake and external carbonic anhydrase. Using the K_m (CO_2) value for type I RubisCO of 17.6 µM CO_2 (see above) and the measured $K_{1/2}$ (CO_2) values (Fig. 6), *K. brevis* must accumulate 13, 11, and 5 times the CO_2 concentration within the proximity of RubisCO compared to the media, leading to a saturation of 67%, 86%, and 86% in the 150, 400, and 780 pCO_2 acclimations, respectively. Most of our calculation is based on a RubisCO Km (CO_2) found for *P. lutheri,* a phylogenetically close relative. *P. lutheri*, however, does not contain pyrenoids and CCM parameters are unknown (Heureux et al., 2017). Consequently, the K_m values in *K. brevis* might be more similar to those of *Emiliania huxleyi* and therefore all assumptions made here have to be taken with caution and accumulation rates are likely higher in *K. brevis*. Nonetheless, the measured $K_{1/2}$ (CO_2) indicates that *K. brevis* employs a CCM, which is actively downregulated under elevated CO_2 concentration with $K_{1/2}$ (CO_2) similar to those measured in the RubisCO type II containing *Alexandrium tamarense* (Eberlein et al., 2014). Data measured in this study also fit well within the conceptual idea that phytoplankton aim to saturate RubisCO with CO_2 between 80 and 90%, if energetically feasible. In terms of carbon preference, *K. brevis* showed

an increasing utilization of CO_2 uptake with increasing pCO_2 (Fig. 6). Hence, our study suggests that *K. brevis* is able to I) overcome low CO_2 levels by switching to a more readily available but more expensive carbon source, which was seen by changes in the f-value in ^{14}C disequilibrium experiments (Fig. 6) and II) downregulate the energetic expense of the CCM once a higher external CO_2 concentration is available. The measured eCA activity likely acts to maintain diffusive CO_2 uptake and reduce the diffusive loss of internal CO_2 as it supports a persistent CO_2 concentration at the cell surface (at a given carbonate chemistry) (Hopkinson et al., 2013; Trimborn et al., 2008). Enhanced eCA activity has also been postulated to help to recover CO_2 which leaks out of the cells as well as regulate the cell surface pH (Trimborn et al., 2008). As dinoflagellates have been shown to leak approximately 50% of the inorganic carbon taken up (Eberlein et al., 2014), eCA could play an important role in C-acquisition and its recovery in *K. brevis*. Internal CA was not specifically measured in this study, but it is very likely that several internal CAs will support the supply of CO_2 for carbon fixation at RubisCO (Ratti et al., 2007). The measured regulation of *K. brevis*' carbon acquisition as well the evidence of pyrenoids found by Monroe et al. (2010) support the conclusion that *K. brevis* maintains an active CCM.

The CO_2 dependent changes in $K_{1/2}$ values, inorganic carbon source preferences, and CA activity are likely reducing the energetic cost of the CCM under high CO_2 (Hopkinson et al., 2011; Kranz et al., 2015). While this down-regulation of the CCM has a potential to increase growth and productivity purely by saving and reallocating energy between metabolic processes, this response has not been shown here and is not always the case (Eberlein et al., 2014; Hopkinson et al., 2014). The slight increase in brevetoxin content cell^{-1} seen in the 780 µatm cultures could be the result of that energy saved from the CCM under high pCO_2 levels, yet, this study lacks the molecular and mechanistic understanding to prove this hypothesis. The overall slow growth rate and low C requirement might indicate that the CCM regulation in *K. brevis* does not save a significant amount of energy, which could explain the moderate metabolic responses to high or low CO_2. While CCMs have an energetic cost associated to the maintenance of the different mechanisms, the CCM overall might actually not be as costly as previously thought (Hopkinson et al., 2014).

5. Conclusions

Our study is the first measuring CCM activity in the ecologically and economically relevant dinoflagellate *K. brevis*. We found evidence for *K. brevis* having an active and efficient CCM, supporting growth, productivity, and brevetoxin production during bloom situations when CO_2 concentrations could be limiting. Additionally, the CCM is down-regulated under enhanced pCO_2 conditions, which led to changes in photophysiology (e.g. enhanced NPQ and τ), This could in turn result in energy reallocation from C-acquisition to other cellular processes. While this energy reallocation is speculative, it demonstrates the importance of investigating underlying processes such as CCMs when aiming to understand the impacts of environmental change on marine phytoplankton The strong CO_2 dependent regulation of the CCM and photophysiology indicates that *K. brevis* possesses mechanisms which can increase the resilience of this species under a range of CO_2 concentrations, especially during bloom conditions and in a future ocean. Our results highlight the possibility that rising pCO_2 levels could result in increased toxicity of *K. brevis* blooms if CO_2 rises even further than the projected value of 780 µatm CO_2. This result, along with evidence for increases in bloom occurrence in a future ocean (Brand and Compton, 2007), show the potential for increased impacts from *K. brevis* both ecologically and economically in a future high CO_2/low pH ocean.

Acknowledgements

We wish to acknowledge the Florida Fish and Wildlife Commission for providing *Karenia brevis* (CCFWC-126). We would also like to thank Thomas Kelly of Florida State University for providing his R-script which assisted in evaluation of the oxygen evolution data. Additionally, we would like to thank Raphael Richardson for his assistance in running the DIC samples. We would also like to thank the reviewers for constructive comments on the manuscript. This research did not receive any specific grant from funding agencies in the public, commercial, or not-for-profit sectors.

Declarations of interest

None.

Appendix A. Supplementary material

Supplementary data to this article can be found online at https://doi.org/10.1016/j.pocean.2019.01.011.

References

Badger, M.R., Andrews, T.J., Whitney, S.M., Ludwig, M., Yellowlees, D.C., Leggat, W., Price, G.D., 1998. The diversity and coevolution of Rubisco, plastids, pyrenoids, and chloroplast-based CO_2-concentrating mechanisms in algae. Can. J. Bot. 76, 1052–1071. https://doi.org/10.1139/b98-074.

Boyd, P.W., Doney, S.C., 2003. The impact of climate change and feedback processes on the ocean carbon cycle. In: Ocean Biogeochemistry. Springer, pp. 157–193.

Brand, L.E., Campbell, L., Bresnan, E., 2012. *Karenia*: The biology and ecology of a toxic genus. Harmful Algae 14, 156–178. https://doi.org/10.1016/j.hal.2011.10.020.

Brand, L.E., Compton, A., 2007. Long-term increase in *Karenia brevis* abundance along the Southwest Florida Coast. Harmful Algae 6, 232–252. https://doi.org/10.1016/j.hal.2006.08.005.

Calabro, K., Guigonis, J.-M., Teyssié, J.-L., Oberhänsli, F., Goudour, J.-P., Warnau, M., Bottein, M.-Y., Thomas, O., 2014. Further Insights into Brevetoxin Metabolism by de Novo Radiolabeling. Toxins 6, 1785–1798. https://doi.org/10.3390/toxins6061785.

Cassell, R.T., Chen, W., Thomas, S., Liu, L., Rein, K.S., 2015. Brevetoxin, the dinoflagellate neurotoxin, localizes to thylakoid membranes and interacts with the light-harvesting complex II (LHCII) of photosystem II. ChemBioChem 16, 1060–1067. https://doi.org/10.1002/cbic.201402669.

Chen, W., Colon, R., Louda, J.W., del Rey, F.R., Durham, M., Rein, K.S., 2018. Brevetoxin (PbTx-2) influences the redox status and NPQ of *Karenia brevis* by way of thioredoxin reductase. Harmful Algae 71, 29–39. https://doi.org/10.1016/j.hal.2017.11.004.

Dickson, A., Millero, F., 1987. A comparison of the equilibrium constants for the dissociation of carbonic acid in seawater media. Deep Sea Res. Part Oceanogr. Res. Pap. 34, 1733–1743.

Dickson, A.G., 1990. Thermodynamics of the dissociation of boric acid in synthetic seawater from 273.15 to 318.15 K. Deep Sea Res. Part Oceanogr. Res. Pap. 37, 755–766.

Eberlein, T., Van de Waal, D.B., Rost, B., 2014. Differential effects of ocean acidification on carbon acquisition in two bloom-forming dinoflagellate species. Physiol. Plant. 151, 468–479. https://doi.org/10.1111/ppl.12137.

Eichner, M., Kranz, S.A., Rost, B., 2014. Combined effects of different CO_2 levels and N sources on the diazotrophic cyanobacterium Trichodesmium. Physiol. Plant. 152, 316–330. https://doi.org/10.1111/ppl.12172.

Errera, R.M., Bourdelais, A., Drennan, M.A., Dodd, E.B., Henrichs, D.W., Campbell, L., 2010. Variation in brevetoxin and brevenal content among clonal cultures of *Karenia brevis* may influence bloom toxicity. Toxicon 55, 195–203. https://doi.org/10.1016/j.toxicon.2009.07.013.

Errera, R.M., Campbell, L., 2011. Osmotic stress triggers toxin production by the dinoflagellate *Karenia brevis*. Proc. Natl. Acad. Sci. 108, 10597–10601. https://doi.org/10.1073/pnas.1104247108.

Errera, R.M., Yvon-Lewis, S., Kessler, J.D., Campbell, L., 2014. Reponses of the dinoflagellate *Karenia brevis* to climate change: pCO2 and sea surface temperatures. Harmful Algae 37, 110–116. https://doi.org/10.1016/j.hal.2014.05.012.

Espie, G.S., Colman, B., 1986. Inorganic carbon uptake during photosynthesis: I. A theoretical analysis using the isotopic disequilibrium technique. Plant Physiol. 80, 863–869. https://doi.org/10.1104/pp.80.4.863.

Fleming, L.E., Backer, L.C., Baden, D.G., 2005. Overview of aerosolized Florida red tide toxins: exposures and effects. Environ. Health Perspect. 618–620.

Flewelling, L.J., Naar, J.P., Abbott, J.P., Baden, D.G., Barros, N.B., Bossart, G.D., Bottein, M.-Y.D., Hammond, D.G., Haubold, E.M., Heil, C.A., et al., 2005. Brevetoxicosis: red tides and marine mammal mortalities. Nature 435, 755–756.

Fu, F., Place, A., Garcia, N., Hutchins, D., 2010. CO2 and phosphate availability control the toxicity of the harmful bloom dinoflagellate Karlodinium veneficum. Aquat. Microb. Ecol. 59, 55–65. https://doi.org/10.3354/ame01396.

Gao, K., Xu, J., Gao, G., Li, Y., Hutchins, D.A., Huang, B., Wang, L., Zheng, Y., Jin, P., Cai, X., Häder, D.-P., Li, W., Xu, K., Liu, N., Riebesell, U., 2012. Rising CO2 and increased light exposure synergistically reduce marine primary productivity. Nat. Clim.

Change. https://doi.org/10.1038/nclimate1507.
Giordano, M., Beardall, J., Raven, J.A., 2005. CO_2 Concentrating mechanisms in algae:-mechanisms, environmental modulation, and evolution. Annu. Rev. Plant Biol. 56, 99–131. https://doi.org/10.1146/annurev.arplant.56.032604.144052.
Glibert, P., Anderson, D., Gentien, P., Granéli, E., Sellner, K., 2005. The global, complex phenomena of harmful algal blooms. Oceanography 18, 136–147. https://doi.org/10.5670/oceanog.2005.49.
Guillard, R.R.L., Ryther, J.H., 1962. Studies of marine planktonic diatoms: I. Cyclotella Nana Hustedt, and Detonula Confervacea (Cleve) Gran. Can. J. Microbiol. 8, 229–239. https://doi.org/10.1139/m62-029.
Hansen, P., Lundholm, N., Rost, B., 2007. Growth limitation in marine red-tide dinoflagellates: effects of pH versus inorganic carbon availability. Mar. Ecol. Prog. Ser. 334, 63–71. https://doi.org/10.3354/meps334063.
Hansen, P.J., 2002. Effect of high pH on the growth and survival of marine phytoplankton: implications for species succession. Aquat. Microb. Ecol. 28, 279–288.
Hardison, D.R., Sunda, W.G., Shea, D., Litaker, R.W., 2013. Increased toxicity of *karenia brevis* during phosphate limited growth: ecological and evolutionary implications. PLoS One 8, e58545. https://doi.org/10.1371/journal.pone.0058545.
Hardison, D.R., Sunda, W.G., Tester, P.A., Shea, D., Litaker, W.R., 2014. Increased cellular brevetoxins in the red tide dinoflagellate *Karenia brevis* under CO2 limitation of growth rate: evolutionary implications and potential effects on bloom toxicity. Limnol. Oceanogr. 59, 560–577. https://doi.org/10.4319/lo.2014.59.2.0560.
Hardison, D.R., Sunda, W.G., Wayne Litaker, R., Shea, D., Tester, P.A., 2012. Nitrogen limitation increases brevetoxins in *Karenia brevis* (Dinophyceae): implications for bloom toxicity. J. Phycol. 48, 844–858. https://doi.org/10.1111/j.1529-8817.2012.01186.x.
Hattenrath-Lehmann, T.K., Smith, J.L., Wallace, R.B., Merlo, L.R., Koch, F., Mittelsdorf, H., Goleski, J.A., Anderson, D.M., Gobler, C.J., 2015. The effects of elevated CO_2 on the growth and toxicity of field populations and cultures of the saxitoxin-producing dinoflagellate, *Alexandrium fundyense*: Effects of elevated CO_2 on *A. fundyense*. Limnol. Oceanogr. 60, 198–214. https://doi.org/10.1002/lno.10012.
Heil, C.A., Dixon, L.K., Hall, E., Garrett, M., Lenes, J.M., O'Neil, J.M., Walsh, B.M., Bronk, D.A., Killberg-Thoreson, L., Hitchcock, G.L., Meyer, K.A., Mulholland, M.R., Procise, L., Kirkpatrick, G.J., Walsh, J.J., Weisberg, R.W., 2014. Blooms of *Karenia brevis* (Davis) G. Hansen & Ø. Moestrup on the West Florida Shelf: nutrient sources and potential management strategies based on a multi-year regional study. Harmful Algae 38, 127–140. https://doi.org/10.1016/j.hal.2014.07.016.
Heureux, A.M.C., Young, J.N., Whitney, S.M., Eason-Hubbard, M.R., Lee, R.B.Y., Sharwood, R.E., Rickaby, R.E.M., 2017. The role of Rubisco kinetics and pyrenoid morphology in shaping the CCM of haptophyte microalgae. J. Exp. Bot. 68, 3959–3969. https://doi.org/10.1093/jxb/erx179.
Hitchcock, G.L., Kirkpatrick, G., Lane, P.V.Z., Langdon, C., 2014. Comparative diel oxygen cycles preceding and during a *Karenia* bloom in Sarasota Bay, Florida, USA. Harmful Algae 38, 95–100. https://doi.org/10.1016/j.hal.2014.05.010.
Hoagland, P., Jin, D., Polansky, L.Y., Kirkpatrick, B., Kirkpatrick, G., Fleming, L.E., Reich, A., Watkins, S.M., Ullmann, S.G., Backer, L.C., 2009. The costs of respiratory illnesses arising from Florida Gulf Coast *Karenia brevis* blooms. Environ. Health Perspect. 117, 1239.
Hoins, M., Eberlein, T., Großmann, C.H., Brandenburg, K., Reichart, G.-J., Rost, B., Sluijs, A., Van de Waal, D.B., 2016. Combined effects of ocean acidification and light or nitrogen availabilities on 13C fractionation in marine dinoflagellates. PLoS One 11, e0154370. https://doi.org/10.1371/journal.pone.0154370.
Hopkinson, B.M., Dupont, C.L., Allen, A.E., Morel, F.M.M., 2011. Efficiency of the CO2-concentrating mechanism of diatoms. Proc. Natl. Acad. Sci. 108, 3830–3837. https://doi.org/10.1073/pnas.1018062108.
Hopkinson, B.M., Meile, C., Shen, C., 2013. Quantification of extracellular carbonic anhydrase activity in two marine diatoms and investigation of its role. Plant Physiol. 162, 1142–1152. https://doi.org/10.1104/pp.113.217737.
Hopkinson, B.M., Young, J.N., Tansik, A.L., Binder, B.J., 2014. The minimal CO2-concentrating mechanism of *Prochlorococcus* spp. MED4 Is effective and efficient. Plant Physiol. 166, 2205–2217. https://doi.org/10.1104/pp.114.247049.
Hutchins, D.A., Fu, F.-X., Webb, E.A., Walworth, N., Tagliabue, A., 2013. Taxon-specific response of marine nitrogen fixers to elevated carbon dioxide concentrations. Nat. Geosci. 6, 790–795. https://doi.org/10.1038/ngeo1858.
Kolber, Z., Falkowski, P.G., 1993. Use of active fluorescence to estimate phytoplankton photosynthesis in situ. Limnol. Oceanogr. 38, 1646–1665.
Kottmeier, D.M., Rokitta, S.D., Tortell, P.D., Rost, B., 2014. Strong shift from HCO3 − to CO2 uptake in Emiliania huxleyi with acidification: new approach unravels acclimation versus short-term pH effects. Photosynth. Res. 121, 265–275. https://doi.org/10.1007/s11120-014-9984-9.
Kranz, S.A., Eichner, M., Rost, B., 2011. Interactions between CCM and N2 fixation in Trichodesmium. Photosynth. Res. 109, 73–84. https://doi.org/10.1007/s11120-010-9611-3.
Kranz, S.A., Young, J.N., Hopkinson, B.M., Goldman, J.A.L., Tortell, P.D., Morel, F.M.M., 2015. Low temperature reduces the energetic requirement for the CO2 concentrating mechanism in diatoms. New Phytol. 205, 192–201. https://doi.org/10.1111/nph.12976.
Landsberg, J.H., 2002. The effects of harmful algal blooms on aquatic organisms. Rev. Fish. Sci. 10, 113–390.
Langer, G., Probert, I., Nehrke, G., Ziveri, P., 2011. The morphological response of Emiliania huxleyi to seawater carbonate chemistry changes: an inter-strain comparison. J. Nannoplankton Res. 32, 29–34.
Lawrenz, E., Silsbe, G., Capuzzo, E., Ylöstalo, P., Forster, R.M., Simis, S.G.H., Prášil, O., Kromkamp, J.C., Hickman, A.E., Moore, C.M., Forget, M.-H., Geider, R.J., Suggett, D.J., 2013. Predicting the electron requirement for carbon fixation in seas and oceans. PLoS One 8, e58137. https://doi.org/10.1371/journal.pone.0058137.
Lekan, D.K., Tomas, C.R., 2010. The brevetoxin and brevenal composition of three *Karenia brevis* clones at different salinities and nutrient conditions. Harmful Algae 9, 39–47. https://doi.org/10.1016/j.hal.2009.07.004.
Losh, J.L., Young, J.N., Morel, F.M.M., 2013. Rubisco is a small fraction of total protein in marine phytoplankton. New Phytol. 198, 52–58. https://doi.org/10.1111/nph.12143.
Mackey, K., Morris, J.J., Morel, F., Kranz, S., 2015. Response of photosynthesis to ocean acidification. Oceanography 25, 74–91. https://doi.org/10.5670/oceanog.2015.33.
Magaña, H.A., Villareal, T.A., 2006. The effect of environmental factors on the growth rate of *Karenia brevis* (Davis) G. Hansen Moestrup. Harmful Algae 5, 192–198. https://doi.org/10.1016/j.hal.2005.07.003.
Maier Brown, A.F., Dortch, Q., Dolah, F.M.V., Leighfield, T.A., Morrison, W., Thessen, A.E., Steidinger, K., Richardson, B., Moncreiff, C.A., Pennock, J.R., 2006. Effect of salinity on the distribution, growth, and toxicity of *Karenia* spp. Harmful Algae 5, 199–212. https://doi.org/10.1016/j.hal.2005.07.004.
Martin, D.F., Carnahan, R.P., Krzanowski, J.J., 2003. Effect of shear forces on the release of brevetoxins from *Karenia brevis*. Fla. Sci. 109–112.
Mehrbach, C., Culberson, C., Hawley, J., Pytkowicx, R., 1973. Measurement of the apparent dissociation constants of carbonic acid in seawater at atmospheric pressure. Limnol. Oceanogr. 18, 897–907.
Monroe, E.A., Johnson, J.G., Wang, Z., Pierce, R.K., Van Dolah, F.M., 2010. Characterization and expression of nuclear-encoded polyketide synthases in the brevetoxin-producing dinoflagellate *Karenia brevis*. J. Phycol. 46, 541–552. https://doi.org/10.1111/j.1529-8817.2010.00837.x.
Moore, S.K., Trainer, V.L., Mantua, N.J., Parker, M.S., Laws, E.A., Backer, L.C., Fleming, L.E., 2008. Impacts of climate variability and future climate change on harmful algal blooms and human health. Environ. Health 7, S4. https://doi.org/10.1186/1476-069X-7-S2-S4.
Morse, D., Salois, P., Markovic, P., Hastings, J., 1995. A nuclear-encoded form II RuBisCO in dinoflagellates. Science 268, 1622–1624. https://doi.org/10.1126/science.7777861.
Noguchi, T., Hatta, M., Yamanaka, T., Okamura, K., 2013. Fast measurement of dissolved inorganic carbon concentration for small-volume interstitial water by acid extraction and nondispersive infrared gas analysis. Anal. Sci. 29, 9–13. https://doi.org/10.2116/analsci.29.9.
Oxborough, K., Moore, C.M., Suggett, D.J., Lawson, T., Chan, H.G., Geider, R.J., 2012. Direct estimation of functional PSII reaction center concentration and PSII electron flux on a volume basis: a new approach to the analysis of Fast Repetition Rate fluorometry (FRRf) data: analysis of FRRf data: a new approach. Limnol. Oceanogr. Methods 10, 142–154. https://doi.org/10.4319/lom.2012.10.142.
Petrou, K., Kranz, S.A., Trimborn, S., Hassler, C.S., Ameijeiras, S.B., Sackett, O., Ralph, P.J., Davidson, A.T., 2016. Southern Ocean phytoplankton physiology in a changing climate. J. Plant Physiol. 203, 135–150. https://doi.org/10.1016/j.jplph.2016.05.004.
Pierce, R.H., Henry, M.S., 2008. Harmful algal toxins of the Florida red tide (*Karenia brevis*): natural chemical stressors in South Florida coastal ecosystems. Ecotoxicology 17, 623–631. https://doi.org/10.1007/s10646-008-0241-x.
Pierrot, D.E., Wallace, D.W.R., Lewis, E., 2011. MS Excel Program Developed for CO2 System Calculations. https://doi.org/10.3334/CDIAC/otg.CO2SYS_XLS_CDIAC105a.
Price, N.M., Harrison, G.I., Hering, J.G., Hudson, R.J., Nirel, P.M.V., Palenik, B., Morel, F.M.M., 1989. Preparation and chemistry of the artificial algal culture medium aquil. Biol. Oceanogr. 6, 443–461. https://doi.org/10.1080/01965581.1988.10749544.
Raateoja, M., Seppälä, J., Kuosa, H., 2004. Bio-optical modelling of primary production in the SW Finnish coastal zone, Baltic Sea: fast repetition rate fluorometry in Case 2 waters. Mar. Ecol. Prog. Ser. 267, 9–26.
Ratti, S., Giordano, M., Morse, D., 2007. CO_2-concentrating mechanisms of the potentially toxic dinoflagellate *Protoceratium Reticulatum* (Dinophyceae, Gonyaulacales). J. Phycol. 43, 693–701. https://doi.org/10.1111/j.1529-8817.2007.00368.x.
Raven, J.A., Giordano, M., Beardall, J., Maberly, S.C., 2012. Algal evolution in relation to atmospheric CO2: carboxylases, carbon-concentrating mechanisms and carbon oxidation cycles. Philos. Trans. R. Soc. B Biol. Sci. 367, 493–507. https://doi.org/10.1098/rstb.2011.0212.
Raven, J.A., Johnston, A.M., 1991. Mechanisms of inorganic-carbon acquisition in marine phytoplankton and their implications for the use of other resources. Limnol. Oceanogr. 36, 1701–1714. https://doi.org/10.4319/lo.1991.36.8.1701.
Rost, B., Kranz, S., Richter, K.-U., Tortell, P.D., 2007. Isotope disequilibrium and mass spectrometric studies of inorganic carbon acquisition by phytoplankton. Limnol. Oceanogr. Methods 5, 328–337.
Rost, B., Zondervan, I., Wolf-Gladrow, D., 2008. Sensitivity of phytoplankton to future changes in ocean carbonate chemistry: current knowledge, contradictions and research directions. Mar. Ecol. Prog. Ser. 373, 227–237. https://doi.org/10.3354/meps07776.
Roth, P.B., Twiner, M.J., Wang, Z., Bottein Dechraoui, M.-Y., Doucette, G.J., 2007. Fate and distribution of brevetoxin (PbTx) following lysis of *Karenia brevis* by algicidal bacteria, including analysis of open A-ring derivatives. Toxicon 50, 1175–1191. https://doi.org/10.1016/j.toxicon.2007.08.003.
Schaum, E., Rost, B., Millar, A.J., Collins, S., 2013. Variation in plastic responses of a globally distributed picoplankton species to ocean acidification. Nat. Clim. Change 3, 298–302. https://doi.org/10.1038/nclimate1774.
Silverman, D.N., 1982. Carbonic anhydrase: oxygen-18 exchange catalyzed by an enzyme with rate-contributing Proton-transfer steps. Methods Enzymol. 87, 732–752.
Solomon, S., Qin, D., Manning, M., Averyt, K., Marquis, M., 2007. Climate Change 2007-the Physical Science Basis: Working Group I Contribution to the Fourth Assessment Report of the IPCC. Cambridge University Press.
Steidinger, K.A., 2009. Historical perspective on *Karenia brevis* red tide research in the Gulf of Mexico. Harmful Algae 8, 549–561.

Stoecker, D.K., Hansen, P.J., Caron, D.A., Mitra, A., 2017. Mixotrophy in the Marine Plankton. Annu. Rev. Mar. Sci. 9, 311–335. https://doi.org/10.1146/annurev-marine-010816-060617.

Sun, J., Hutchins, D.A., Feng, Y., Seubert, E.L., Caron, D.A., Fu, F.-X., 2011. Effects of changing p CO $_2$ and phosphate availability on domoic acid production and physiology of the marine harmful bloom diatom *Pseudo-nitzschia multiseries*. Limnol. Oceanogr. 56, 829–840. https://doi.org/10.4319/lo.2011.56.3.0829.

Tatters, A.O., Flewelling, L.J., Fu, F., Granholm, A.A., Hutchins, D.A., 2013. High CO2 promotes the production of paralytic shellfish poisoning toxins by Alexandrium catenella from Southern California waters. Harmful Algae 30, 37–43. https://doi.org/10.1016/j.hal.2013.08.007.

Tatters, A.O., Fu, F.-X., Hutchins, D.A., 2012. High CO2 and Silicate Limitation Synergistically Increase the Toxicity of Pseudo-nitzschia fraudulenta. PLoS One 7, e32116. https://doi.org/10.1371/journal.pone.0032116.

Tortell, P.D., 2000. Evolutionary and ecological perspectives on carbon acquisition in phytoplankton. Limnol. Oceanogr. 45, 744–750. https://doi.org/10.4319/lo.2000.45.3.0744.

Tortell, P.D., Trimborn, S., Li, Y., Rost, B., Payne, C.D., 2010. Inorganic carbon utilization by Ross Sea phytoplankton across natural and experimental CO2 gradients. J. Phycol. 46, 433–443.

Trimborn, S., Lundholm, N., Thoms, S., Richter, K.-U., Krock, B., Hansen, P.J., Rost, B., 2008. Inorganic carbon acquisition in potentially toxic and non-toxic diatoms: the effect of pH-induced changes in seawater carbonate chemistry. Physiol. Plant. 133, 92–105. https://doi.org/10.1111/j.1399-3054.2007.01038.x.

Uppström, L.R., 1974. The boron/chlorinity ratio of deep-sea water from the Pacific Ocean. In: Deep Sea Research and Oceanographic Abstracts. Elsevier, pp. 161–162.

van de Waal, D.B., Eberlein, T., Bublitz, Y., John, U., Rost, B., 2014. Shake it easy: a gently mixed continuous culture system for dinoflagellates. J. Plankton Res. 36, 889–894. https://doi.org/10.1093/plankt/fbt138.

Van Dolah, F.M., Lidie, K.B., Monroe, E.A., Bhattacharya, D., Campbell, L., Doucette, G.J., Kamykowski, D., 2009. The Florida red tide dinoflagellate *Karenia brevis*: new insights into cellular and molecular processes underlying bloom dynamics. Harmful Algae 8, 562–572. https://doi.org/10.1016/j.hal.2008.11.004.

Van Dolah, F.M., Lidie, K.B., Morey, J.S., Brunelle, S.A., Ryan, J.C., Monroe, E.A., Haynes, B.L., 2007. Microarray analysis of diurnal- and circadian-regulated genes in the Florida red-tide dinoflagellate *Karenia brevis* (Dinophyceae). J. Phycol. 43, 741–752. https://doi.org/10.1111/j.1529-8817.2007.00354.x.

Wiliams, P.J.L., Robertson, J.E., 1991. Overall planktonic oxygen and carbon dioxide metabolisms: the problem of reconciling observations and calculations of photosynthetic quotients. J. Plankton Res. https://doi.org/10.1093/oxfordjournals.plankt.a042366.

Wu, Y., Gao, K., Riebesell, U., 2010. CO2-induced seawater acidification affects physiological performance of the marine diatom Phaeodactylum tricornutum. Biogeosciences 7, 2915–2923. https://doi.org/10.5194/bg-7-2915-2010.

Yang, G., Gao, K., 2012. Physiological responses of the marine diatom Thalassiosira pseudonana to increased pCO2 and seawater acidity. Mar. Environ. Res. 79, 142–151. https://doi.org/10.1016/j.marenvres.2012.06.002.

Yoon, H.S., Hackett, J.D., Bhattacharya, D., 2002. A single origin of the peridinin- and fucoxanthin-containing plastids in dinoflagellates through tertiary endosymbiosis. Proc. Natl. Acad. Sci. 99, 11724–11729. https://doi.org/10.1073/pnas.172234799.

Yoon, H.S., Hackett, J.D., Van Dolah, F.M., Nosenko, T., Lidie, K.L., Bhattacharya, D., 2005. Tertiary endosymbiosis driven genome evolution in dinoflagellate algae. Mol. Biol. Evol. 22, 1299–1308.

Zhang, H., Byrne, R.H., 1996. Spectrophotometric pH measurements of surface seawater at in-situ conditions: absorbance and protonation behavior of thymol blue. Mar. Chem. 52, 17–25. https://doi.org/10.1016/0304-4203(95)00076-3.